Directed Graph Dynamic Mode Decomposition for Nonlinear State-Space Modeling

Hiromu Kanauchi*, Ryuto Ito*, Hiroyasu Yasuda*, Masaaki Nagahara†,
Yuichi Tanaka‡, and Shogo Muramatsu*
* Niigata University, Niigata, Japan
E-mail: kurou1315@gmail.com; itory0214@gmail.com; hiro@gs.niigata-u.ac.jp; shogo@eng.niigata-u.ac.jp
† Hiroshima University, Hiroshima, Japan
E-mail: nagahara@ieee.org
‡ The University of Osaka, Osaka, Japan
E-mail: ytanaka@comm.eng.osaka-u.ac.jp

***Abstract*—This paper proposes a directed graph filter bank for predicting river water level distributions using time-delay dynamic mode decomposition (tdDMD) and sparse modeling. The previously proposed sparse-coded time-delay graph dynamic mode decomposition (STG-DMD) derived time evolution equations from water level data on an undirected graph structure, achieving high-accuracy predictions by considering multiple location connections. However, because the connections were defined as undirected graphs, the river flow direction was not considered. Therefore, this paper aims to incorporate river flow direction using a directed graph structure. To verify the effectiveness of the proposed method, performance evaluation experiments were conducted using both artificial and real observation data. The reproducibility of the proposed method was evaluated using water level data generated by process-driven models. In the experiment, water level data were collected via web scraping from the Internet, and river water level distribution was predicted. The results of the performance evaluations demonstrate that the proposed method outperforms STG-DMD.**

I. Introduction

Severe floods are becoming increasingly frequent worldwide [1], [2]. In Japan, flood-related events such as the torrential rains in August 2022 and July 2023 have revealed the limitations of current flood control technologies. In 2020, the Ministry of Land, Infrastructure, Transport and Tourism (MLIT) of Japan introduced the "River Basin Disaster Resilience and Sustainability by All" policy[1], promoting integrated flood management through drainage, detours, and water storage. To realize this policy, river basins can be regarded as large-scale networks in which numerous tributaries are interconnected as a directed graph (digraph), enabling the monitoring of water levels throughout the river system. However, conventional flood prediction models treat each observation point independently in time series modeling, neglecting spatial directions and thus failing to capture local error propagation. In fact, Singh *et al.* [3] reported that, for a single river channel, a linear approximation of the nonlinear dynamics keeps water level errors within approximately ±10%. In contrast, David *et al.* [4] analytically demonstrated that in large-scale river systems, small upstream errors can accumulate and interact through the network, amplifying to several tens of percent downstream. These findings strongly suggest the need for modeling approaches that simultaneously capture spatial topology and nonlinearity.

To address this, data-driven approaches that utilize the river network structure have been gaining attention. For example, Arai *et al.* proposed sparse-coded dynamic mode decomposition on graph (SC-DMD-G) [5], which derives time evolution equations from water level data on undirected graphs by integrating extended dynamic mode decomposition (eDMD) [6], [7] and a graph filter bank (GFB) [8], [9] as a sparse approximation dictionary. Building on this foundation, Ito *et al.* proposed sparse-coded time-delay graph dynamic mode decomposition (STG-DMD) [10], [11], which enables high-accuracy linear modeling of nonlinear dynamical systems such as rivers by incorporating the time-delay dynamic mode decomposition (tdDMD) [12] framework into SC-DMD-G. However, STG-DMD could not incorporate river flow directions because of its use of an undirected graph structure.

To tackle the above-mentioned challenges, this paper derives time evolution equations on a digraph reflecting river flow directions. Graph operators of the digraph are asymmetric, offering no guarantee of diagonalizability. Therefore, the conventional graph Fourier transform (GFT), designed for undirected graphs, cannot be directly applied. To address this problem, various candidate approaches specific to digraphs are explored in this research field.

For example, Furutani *et al.* redefined graph operators as Hermitian symmetric matrices, enabling real-valued graph frequency sorting and realizing filtering in the graph frequency domain [13]. However, it leads to complex-valued outputs despite real-valued inputs. To overcome this issue, Kitamura *et al.* proposed the augmented GFT (AuGFT)[2] [14], which generalizes the traditional GFT and ensures real-valued outputs with filters designed under little constraint. In parallel, Kwak *et al.* applied polar decomposition to the adjacency matrix and

[1] https://www.mlit.go.jp/river/kokusai/pdf/pdf21.pdf

[2] AuGFT https://github.com/msiplab/AuGFT

979-8-3315-7206-8/25/$31.00

introduced a new filtering technique in the vertex domain [15]. Both methods support practical real-valued filtering, but we adopt AuGFT for its advantage of allowing direct utilization of existing filters for undirected graph signals.

Building on this foundation, we propose digraph dynamic mode decomposition (DiGraph-DMD) that incorporates digraph structures and digraph filtering using AuGFT into STG-DMD. This integration enables the derivation of time evolution equations that consider the flow direction of rivers. The effectiveness of DiGraph-DMD is demonstrated through experiments on both artificial and real observation data.

The contributions of this paper are summarized as follows:

- Incorporation of digraph structures and digraph filtering using AuGFT into STG-DMD, enabling the derivation of time evolution equations that reflect the flow direction of rivers.
- Unification of sparse representation on directed graphs, time-delay embedding, and dynamical system modeling in a single data-driven framework.

The remainder of this paper is organized as follows. In Section II, we review the digraph signal processing and STG-DMD. In Section III, we propose DiGraph-DMD. In Section IV, the effectiveness of DiGraph-DMD is evaluated through two types of experiments. Section V concludes the paper and discusses future directions.

II. Review of Digraph Signal Processing and STG-DMD

This section provides an overview of digraph signal processing proposed in [13], [14], [16], and STG-DMD [10], [11].

A. Digraph Signal Processing

A digraph is defined as $\mathcal{G} = \{\mathcal{V}, \mathbf{A}\}$, where $\mathcal{V} \subset \mathbb{N}_0$ is a vertex set, $\mathbf{A} = (a_{m,n}) \in [0,\infty)^{N\times N}$ is an adjacency matrix, $a_{m,n}$ is a weight from vertex m to vertex n, and $N = |\mathcal{V}| < \infty$ is the number of vertices. If $a_{m,n} = a_{n,m}$ holds for all $(m,n) \in \mathcal{V}\times\mathcal{V}$, $\mathcal{G}$ is undirected and $\mathbf{A}$ is symmetric, that is, $\mathbf{A}^\intercal = \mathbf{A}$, where $\intercal$ denotes a transpose of matrix. To ensure that the eigenvalues remain real-valued, a Hermitian adjacency matrix is used, defined by

$$\mathbf{C} = \mathbf{A}_+ + \mathrm{j}\mathbf{A}_- \tag{1}$$

where $\mathbf{A}_+ \coloneqq \frac{1}{2}(\mathbf{A} + \mathbf{A}^\intercal)$, $\mathbf{A}_- \coloneqq \frac{1}{2}(\mathbf{A} - \mathbf{A}^\intercal)$ are the symmetric and skew-symmetric part of $\mathbf{A}$ [13], [14].

In [14], the para-graph Laplacian

$$\mathbf{L} = \mathbf{D} - \mathbf{C} = (\mathbf{D} - \mathbf{A}_+) - \mathrm{j}\mathbf{A}_- \tag{2}$$

is defined based on the Hermitian adjacency matrix, where $\mathbf{D}$ is a degree matrix of $\mathbf{C} = (c_{m,n})$ with diagonal elements defined by

$$d_{m,m} \coloneqq \sum_{n\in\mathcal{V}\setminus\{m\}} \sqrt{c_{m,n}c_{n,m}},\ m \in \mathcal{V}. \tag{3}$$

$\mathbf{L}$ satisfies the Hermitian symmetric property, that is, $\mathbf{L}^\mathsf{H} = \mathbf{L}$, where H denotes the Hermitian transpose of a matrix. For an undirected graph, $\mathbf{C} = \mathbf{A}$, and $\mathbf{L}$ reduces to the conventional graph Laplacian.

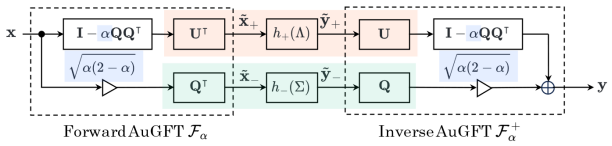

Fig. 1. Digraph filtering $\mathbf{y} = \mathbf{H}\mathbf{x}$ using AuGFT. $\mathbf{U} \in \mathbb{R}^{N\times N}$ and $\mathbf{\Lambda} \in \mathbb{R}^{N\times N}$ are the orthonormal and diagonal matrices obtained from the eigenvalue decomposition of $\Re\{\mathbf{L}\}$, and $\mathbf{Q} \in \mathbb{R}^{N\times r}$ and $\mathbf{\Sigma} \in \mathbb{R}^{r\times r}$ are the orthonormal and block-diagonal matrices obtained from the eigenvalue decomposition of $\Im\{\mathbf{L}\}$. The parameter α controls the skew intensities.

$\mathbf{L}$ can be represented as

$$\mathbf{L} = \mathbf{U}\mathbf{\Lambda}\mathbf{U}^\intercal + \mathrm{j}\mathbf{Q}\mathbf{\Sigma}\mathbf{Q}^\intercal, \tag{4}$$

where $\mathbf{U} \in \mathbb{R}^{N\times N}$ is an orthonormal matrix and $\mathbf{Q} \in \mathbb{R}^{N\times r}$ is a matrix consists of r orthonormal column vectors [14]. The matrices $\mathbf{\Lambda}$ and $\mathbf{\Sigma}$ represent the graph frequencies and skew intensities, respectively:

$$\mathbf{\Lambda} = \mathrm{diag}(\lambda_0, \lambda_1, \cdots, \lambda_{N-1}), \tag{5}$$

$$\mathbf{\Sigma} = s_0 \begin{pmatrix} 0 & 1 \\ -1 & 0 \end{pmatrix} \oplus s_1 \begin{pmatrix} 0 & 1 \\ -1 & 0 \end{pmatrix} \oplus \cdots s_{\frac{r}{2}-1} \begin{pmatrix} 0 & 1 \\ -1 & 0 \end{pmatrix}, \tag{6}$$

where $\lambda_n \in [0,\infty)$, $\lambda_n \le \lambda_m$ for $n < m$, and $s_n \in [0,\infty)$, $s_n \ge s_m$ for $n < m$. The operator $\Im\{\cdot\}$ denotes the imaginary part, and r is the rank of $\Im\{\mathbf{L}\}$. The symbol $\oplus$ denotes the direct sum of matrices to construct a block diagonal matrix.

Let the signal at vertex n be denoted by $x_n \in \mathbb{R}$, then the digraph signal $\{x_n\}_n$ is expressed as $\mathbf{x} = (x_0, x_1, \cdots, x_{N-1})^\intercal \in \mathbb{R}^N$. AuGFT and its left inverse transform (IAuGFT) are defined as

$$\tilde{\mathbf{x}} = \mathcal{F}_\alpha\mathbf{x} \coloneqq \left((\mathbf{I} - \alpha\mathbf{Q}\mathbf{Q}^\intercal)\,\mathbf{U} \quad \sqrt{\alpha(2-\alpha)}\mathbf{Q}\right)^\intercal \mathbf{x}, \tag{7}$$

$$\mathbf{x} = \mathcal{F}_\alpha^+\tilde{\mathbf{x}} \coloneqq \left((\mathbf{I} - \alpha\mathbf{Q}\mathbf{Q}^\intercal)\,\mathbf{U} \quad \sqrt{\alpha(2-\alpha)}\mathbf{Q}\right)\tilde{\mathbf{x}}, \tag{8}$$

where $\tilde{\mathbf{x}} \in \mathbb{R}^{N+r}$, $r = \mathrm{rank}(\Im\{\mathbf{L}\})$, and $\alpha \in [0,1]$ [16]. α is the parameter that controls the skew intensities.

In the filtering approach adopted in this paper via AuGFT/IAuGFT, a real input produces a real-valued output [14]. In the transform domain via AuGFT, a digraph filter can be defined as

$$\mathbf{y} = \mathbf{H}\mathbf{x}, \tag{9}$$

where $\mathbf{y} \in \mathbb{R}^N$ is the filtered digraph signal, and $\mathbf{H} \in \mathbb{R}^{N\times N}$ is the filter in the vertex domain. Fig. 1 shows the procedure of digraph filtering. The vertex-domain filter $\mathbf{H}$ in (9) is formulated as

$$\mathbf{H} = \mathcal{F}_\alpha^+ \left(h_+(\mathbf{\Lambda}) \oplus h_-(\mathbf{\Sigma})\right)\mathcal{F}_\alpha, \tag{10}$$

where $h_+(\mathbf{\Lambda})$ and $h_-(\mathbf{\Sigma})$ are defined respectively as

$$h_+(\mathbf{\Lambda}) \coloneqq \mathrm{diag}\left(h_+(\lambda_0), h_+(\lambda_1), \cdots, h_+(\lambda_{N-1})\right), \quad (11)$$

$$h_-(\mathbf{\Sigma}) \coloneqq h_-(s_0)\begin{pmatrix} 0 & 1 \\ -1 & 0 \end{pmatrix} \oplus h_-(s_1)\begin{pmatrix} 0 & 1 \\ -1 & 0 \end{pmatrix} \oplus \cdots$$
$$\cdots \oplus h_-(s_{\frac{r}{2}-1})\begin{pmatrix} 0 & 1 \\ -1 & 0 \end{pmatrix}. \quad (12)$$

As long as both $h_+(\cdot)$ and $h_-(\cdot)$ are designed as real functions, the resulting filter $\mathbf{H}$ is guaranteed to be real.

We consider constructing a P-channel directed GFB $\mathbf{G} = \begin{bmatrix}\mathbf{H}_0 & \mathbf{H}_1 & \cdots & \mathbf{H}_{P-1}\end{bmatrix}$ via dictionary learning [16]. The filters are parameterized using α_p of the p-th filter $\mathbf{H}_p$, and $\mathbf{G}$ is optimized through a dictionary learning method. To learn a P-channel GFB from training data, we formulate the following optimization problem:

$$\{\hat{\mathbf{G}}, \hat{\mathbf{X}}\} = \arg\min_{\{\mathbf{G},\mathbf{X}\}} \frac{1}{2}\|\mathbf{V} - \mathbf{G}\mathbf{X}\|_{\mathrm{F}}^2 + \beta \sum_k \|\mathbf{x}_k\|_1, \quad (13)$$

where $\mathbf{V}$ is the data matrix of graph signals, $\mathbf{X}$ is the coefficient matrix corresponding to $\mathbf{G}$, $\beta \in [0, \infty)$ is a regularization parameter, $\mathbf{x}_k$ is the k-th column vector of $\mathbf{X}$, and $\|\cdot\|_{\mathrm{F}}$ and $\|\cdot\|_1$ denote the Frobenius norm and ℓ_1-norm, respectively. Using (13), the directed GFB is designed.

B. STG-DMD

STG-DMD combines tdDMD with a GFB to derive time evolution equations for water level data on an undirected graph $\mathcal{G}_*$ in a data-driven manner [10], [11]. STG-DMD assumes a linear time-invariant system. tdDMD is used to decompose temporally varying feature vectors into spatiotemporal modes, while a GFB extracts features from vertex signals on $\mathcal{G}_*$. In STG-DMD, sparse approximation is employed to map data from the state space $\mathcal{M} \subseteq \mathbb{R}^M$ to the feature space $\tilde{\mathcal{F}} \subseteq \mathbb{R}^L$, where M and L are the vector dimensions, satisfying $M \leq L$.

Assuming that a graph Laplacian $\mathbf{L}$ and a GFB $\mathbf{G}$ are given in undirected graph signal processing, the time evolution equation on $\mathcal{G}_*$ is obtained by

$$\mathbf{x}(t) = \mathbf{G}\mathbf{P}\mathbf{\Phi}e^{\mathbf{\Omega}t}\mathbf{b}_0 \quad (14)$$

through STG-DMD, where $\mathbf{P} \in \mathbb{R}^{L \times Ld}$ is a projection matrix, and $\mathbf{\Phi}$ is the dynamic modes. In addition, $\mathbf{\Omega} = \ln \mathbf{\Gamma}/\Delta t$ and $\mathbf{b}_0 = \mathbf{\Phi}^\dagger \mathbf{h}_0$, where $\mathbf{\Gamma}$ consists of the eigenvalues on its diagonal, $\dagger$ denotes the Moore–Penrose pseudoinverse, and $\mathbf{h}_k$ is the k-th column of delay-embedded Hankel matrix.

STG-DMD assumes an undirected graph. Even when targeting networks such as rivers that contain directional flow, the directionality of flow is not considered.

III. Digraph Dynamic Mode Decomposition

This section proposes digraph dynamic mode decomposition (DiGraph-DMD) to derive time evolution equations for water level distributions on digraph structures. The framework of DiGraph-DMD is shown in Fig. 2. In STG-DMD, the graph is an undirected graph $\mathcal{G}_*$ and therefore, the synthesis dictionary $\mathbf{G}$ is designed for the undirected setting. In contrast, DiGraph-DMD uses a digraph $\mathcal{G}$ for training a GFB $\hat{\mathbf{G}}$ for the digraph

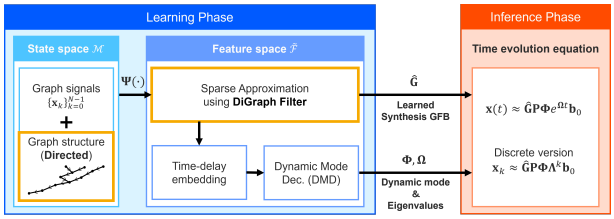

Fig. 2. Framework of DiGraph-DMD. $\{\mathbf{x}_k\}_{k=0}^{N-1}$ is the time series of observed water level data, $\mathbf{\Psi} : \mathcal{M} \to \tilde{\mathcal{F}}$ performs sparse coding, $\hat{\mathbf{G}}$ is a synthesis GFB obtained via digraph dictionary learning, $\mathbf{\Phi}$ is a dynamic mode, $\mathbf{\Omega}$ and $\mathbf{\Lambda}$ are eigenvalue diagonal matrices in the continuous and discrete domain, respectively. $\mathbf{P} \in \mathbb{R}^{L \times Ld}$ is a projection matrix, and $\mathbf{b}_0 = \mathbf{\Phi}^\dagger \mathbf{h}_0$.

setting. By introducing $\mathcal{G}$ and $\hat{\mathbf{G}}$, it becomes possible to derive a time-evolution equation that reflects the flow direction in the river network as a digraph structure.

The time-evolution equation in DiGraph-DMD is expressed as

$$\mathbf{x}(t) = \hat{\mathbf{G}}\mathbf{P}\mathbf{\Phi}e^{\mathbf{\Omega}t}\mathbf{b}_0. \quad (15)$$

The data-driven procedure for deriving the time-evolution equation in DiGraph-DMD is outlined as follows.

1) Prepare a training dataset of graph signals $\{\mathbf{x}_k\}_{k=0}^{N-1} \subset \mathcal{M}$.
2) Design a P-channel directed GFB $\hat{\mathbf{G}}$ through dictionary learning.
3) Map each signal $\{\mathbf{x}_k\}_{k=0}^{N-1}$ to a feature vector $\{\mathbf{y}_k\}_{k=0}^{N-1} \subset \tilde{\mathcal{F}}$ using a mapping $\mathbf{\Psi}(\cdot)$.
4) Apply time-delay embedding to the sparse coefficient $\mathbf{y}_k$ in the feature space $\tilde{\mathcal{F}}$. This yields a delay-embedded Hankel matrix

$$\mathbf{Y} = \begin{bmatrix} \mathbf{y}_0 & \mathbf{y}_1 & \cdots & \mathbf{y}_{(N-1)-d} \\ \mathbf{y}_1 & \mathbf{y}_2 & \cdots & \mathbf{y}_{(N-1)-d+1} \\ \vdots & \vdots & \ddots & \vdots \\ \mathbf{y}_{d-1} & \mathbf{y}_d & \cdots & \mathbf{y}_{N-2} \end{bmatrix}$$
$$= \begin{bmatrix} | & | & & | \\ \mathbf{h}_0 & \mathbf{h}_1 & \cdots & \mathbf{h}_{(N-1)-d} \\ | & | & & | \end{bmatrix} \in \mathbb{R}^{(Ld)\times(N-d)}, \quad (16)$$

where d is the number of time delays.
5) In the feature space $\tilde{\mathcal{F}}$, derive a linear operator $\mathbf{K}$ that approximates the time evolution of $\mathbf{h}_k$ as $\mathbf{h}_k \simeq \mathbf{K}\mathbf{h}_{k-1}$.
6) Use DMD [17], [18] to compute the dynamic modes $\mathbf{\Phi}$ and eigenvalues $\mathbf{\Gamma}$.

The coefficient and dictionary update steps of the dictionary learning for designing $\hat{\mathbf{G}}$ using (13) are shown below:

- Coefficient update step: given the dictionary $\mathbf{G}_{\hat{\theta}}$, which is either the initial state or the result from the previous step, update the coefficients

$$\hat{\mathbf{X}} = \arg\min_{\mathbf{X}} \frac{1}{2}\|\mathbf{V} - \mathbf{G}_{\hat{\theta}}\mathbf{X}\|_{\mathrm{F}}^2 + \beta \sum_k \|\mathbf{x}_k\|_1, \quad (17)$$

where $\mathbf{G}_{\hat{\theta}}$ is the GFB defined by the design parameter $\hat{\theta}$.

- Dictionary update step: given the coefficient $\hat{\mathbf{X}}$ from the previous step, update the design parameter

$$\hat{\theta} = \arg\min_{\theta} \frac{1}{2}\|\mathbf{V} - \mathbf{G}_{\theta}\hat{\mathbf{X}}\|_{\mathrm{F}}^2. \tag{18}$$

Given $\hat{\mathbf{G}}$, the sparse coding $\mathbf{\Psi}(\cdot)$ is defined as

$$\mathbf{\Psi}(\mathbf{x}) = \arg\min_{\mathbf{y}\in\mathbb{R}^L} \frac{1}{2}\|\mathbf{x} - \hat{\mathbf{G}}\mathbf{y}\|_2^2 + \epsilon\rho(\mathbf{y}), \tag{19}$$

where $\epsilon \in [0, \infty)$ is a regularization parameter. For $\rho(\cdot) = \|\cdot\|_1$, ISTA [19] updates $\mathbf{y}^{(i)}$ from $\mathbf{y}^{(0)}$ as

$$\mathbf{y}^{(i+1)} \leftarrow \mathcal{T}_{\gamma\epsilon}\left(\mathbf{y}^{(i)} - \gamma\hat{\mathbf{G}}^{\mathsf{T}}(\hat{\mathbf{G}}\mathbf{y}^{(i)} - \mathbf{x})\right), \tag{20}$$

$$i \leftarrow i + 1, \tag{21}$$

where $\hat{\mathbf{G}}^{\mathsf{T}}$ is the adjoint of $\hat{\mathbf{G}}$, and $\mathcal{T}_{\gamma\epsilon}(\cdot)$ is the soft-thresholding operator with step size γ.

Note that setting $\alpha_p = 0$ reduces the proposed method to the conventional STG-DMD, serving as a special case of the proposed framework.

IV. Performance Evaluation

In this section, two types of experiments are conducted using artificial and real observation data to evaluate the performance of the proposed DiGraph-DMD. In both experiments, the frequency response of the p-th filter $\{h_{p,+}(\cdot)\}$ uses a half-cosine GFB, provided by GSPBox[3], and the skew response of the p-th filter $\{h_{p,-}(\cdot)\}$ is fixed as $h_{p,-}(s) = 1$.

A. Reproduction Experiment

In this experiment, water level datasets are generated using tank models, which are process-driven models based on physical first principles. The water levels obtained from the derived time evolution equations by STG-DMD and DiGraph-DMD are compared with those obtained from the nonlinear state equations of the tank models, and the reproduction errors are evaluated.

In this experiment, two tank models are used, referred to as follows:

[3]GSPBox https://epfl-lts2.github.io/gspbox-html/

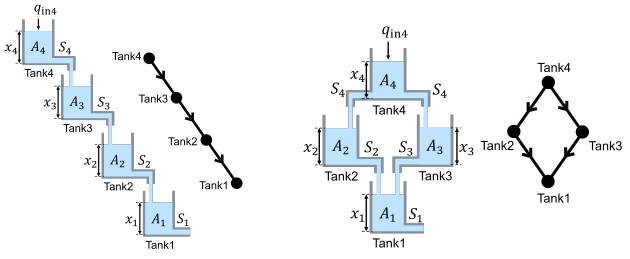

(a) Series tank model (b) Parallel tank model

Fig. 3. Schematic diagrams of the series and parallel tank models. x_i is the water level of the tank, A_i and S_i are the cross-sectional areas of the tank and outlet, respectively, and $q_{\mathrm{in},i}$ is the inflow. The subscript numbers represent the tank numbers. The digraph on the right represents the digraph structure of each tank model.

TABLE I
Parameter setup of the tank models

Tank ID: i	1	2	3	4
Initial water level $x_{0,i}$ [m]	10			
Tank cross-sectional area A_i [m^2]	30			
Outlet cross-sectional area S_i [m^2]	0.003			
Inflow rate $q_{\mathrm{in},i}$ [m^3/s]	0			
Gravitational acceleration g [m/s^2]	9.81			
Simulation time t [s]	43200			
Sampling interval Δt [s]	600			

TABLE II
GFB design setup for reproduction experiment

Tank model	Series	Parallel
Number of data for dictionary learning	4×73	4×73
Filter for $h_{p,+}(\cdot)$	Half cosine	Half cosine
Number of filters P	8	8
Reg. Param. of ISTA β	7.0×10^{-2}	4.0×10^{-2}
Reg. Param. of ISTA ϵ	1.0×10^{-4}	1.0×10^{-6}

- Series tank model: A model in which four tanks are connected in series.
- Parallel tank model: A model in which four tanks are connected in parallel.

Schematic diagrams of the two tank models are shown in Fig. 3. The parameter values of the tank models are shown in Table I. In addition, the design specifications of the GFB used in DiGraph-DMD is shown in Table II. The projection matrix $\mathbf{P}$ given in (15) is set as $\begin{bmatrix}\mathbf{I} & \mathbf{O} & \cdots & \mathbf{O}\end{bmatrix}$, where $\mathbf{I}$ is the identity matrix and $\mathbf{O}$ is the zero matrix.

The reproduction results of water levels and the corresponding error evaluations at each time step for tank 3 of the series tank model and tank 4 of the parallel tank model are shown in Fig. 4. In addition, the root mean square error (RMSE)

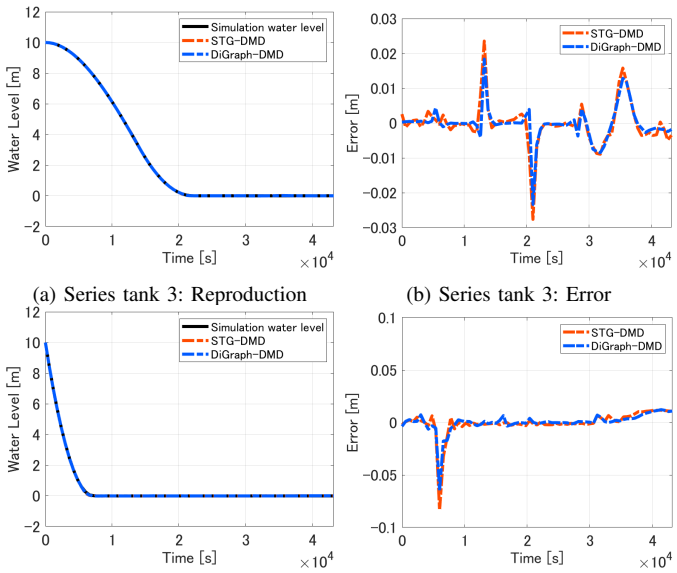

(a) Series tank 3: Reproduction (b) Series tank 3: Error

(c) Parallel tank 4: Reproduction (d) Parallel tank 4: Error

Fig. 4. Reproduction results and corresponding errors for tank 3 of the series tank model and tank 4 of the parallel tank model.

TABLE III
RMSE FOR EACH TANK MODEL

Tank	STG-DMD [m]	DiGraph-DMD [m]
Series tank model		
Tank1	**0.0073**	0.0074
Tank2	0.0086	**0.0084**
Tank3	0.0060	**0.0049**
Tank4	0.0062	**0.0061**
Parallel tank model		
Tank1	**0.0083**	0.0103
Tank2	0.0042	**0.0040**
Tank3	0.0042	**0.0040**
Tank4	0.0118	**0.0093**

TABLE IV
PREDICTION EXPERIMENTAL SETUP

Observation period	April 6 to April 10, 2022 (JST) April 19 to April 23, 2022 (JST) May 17 to May 21, 2022 (JST)
Training period	April 6 at 1 a.m. to April 9 at 12 p.m. April 19 at 1 a.m. to April 22 at 12 p.m. May 17 at 1 a.m. to May 20 at 12 p.m.
Prediction period	April 10 at 1 a.m. to 12 p.m. April 23 at 1 a.m. to 12 p.m. May 21 at 1 a.m. to 12 p.m.
Meas. interval Δt [h]	1
Number of observation points	40
Number of delay	24

TABLE V
GFB DESIGN SETUP FOR PREDICTION EXPERIMENT

Number of data for dictionary learning	40×96
Filter for $h_{p,+}(\cdot)$	Half cosine
Number of filters P	8
Reg. Param. of ISTA β	1.0×10^{-3}
Reg. Param. of ISTA ϵ	9.5×10^{-3}

calculated over the entire simulation period is presented in Table III. These results confirm that the proposed DiGraph-DMD has a reproduction performance superior to that of the conventional STG-DMD.

B. Prediction Experiment

In this experiment, we focused on the Shinano River system, the longest river system in Japan, to derive time evolution equations for water level distributions. These equations were then applied to predict water level distributions across multiple locations in the river network. The water level data used in the experiment were collected through web scraping from publicly available online information. The experimental specifications are shown in Table IV. Because STG-DMD and DiGraph-DMD target autonomous systems, data from periods with little rainfall were extracted to eliminate the influence of external inputs.

The observed water levels, originally in terms of elevation, were centralized to eliminate large absolute values relative to their changes and used as the state vectors $\mathbf{x}_k$.

The digraph structure was defined based on river data from the National Land Numerical Information dataset published by MLIT of Japan. The defined digraph structure is shown in Fig. 5. The design specifications of the GFB constructed through digraph dictionary learning are shown in Table V.

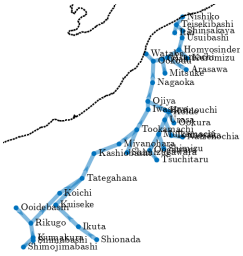

Fig. 5. Digraph $\mathcal{G}$ ($N = 40$) of water level observation stations in the Shinano River system. Blue dots represent water level observation stations, and blue lines represent river channels between stations. The digraph uses edge weights of 1 to indicate connections and flow directions.

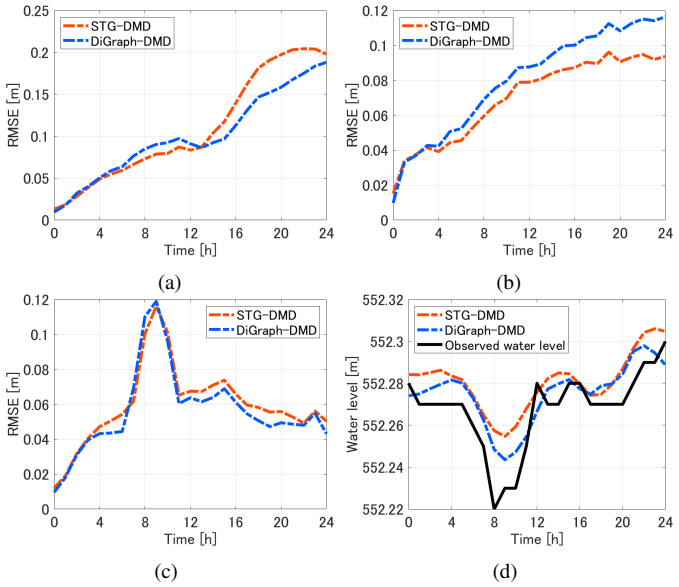

Fig. 6. (a)-(c) RMSE results at all stations during each prediction period: (a) April 10, 1 a.m. to 12 p.m., (b) April 23, 1 a.m. to 12 p.m., (c) May 21, 1 a.m. to 12 p.m. (d) Predicted water levels at the Kumakura observation station for May 21, 1 a.m. to 12 p.m.

The projection matrix $\mathbf{P}$ given in (15) is set as $\begin{bmatrix}\mathbf{O} & \mathbf{O} & \cdots & \mathbf{I}\end{bmatrix}$. In the prediction experiment, the extraction positions were modified from those used in the reproduction experiment to satisfy causality.

Fig. 6(a)–(c) presents the RMSE values across all locations for each prediction period. Fig. 6(d) presents the predicted water level results at the Kumakura observation station. From these results, it is evident that the proposed DiGraph-DMD achieves lower prediction errors and outperforms STG-DMD in terms of predictive accuracy.

V. CONCLUSION

This paper proposes DiGraph-DMD for deriving time-evolution equations of water levels on digraphs. To verify the effectiveness of the proposed method, we conducted reproduction and prediction experiments. The results demonstrated that the proposed DiGraph-DMD not only achieves superior

reproducibility compared to the existing STG-DMD but also improves predictive performance.

As future work, we plan to improve the dictionary $\hat{\mathbf{G}}$ by optimizing both of the filters $h_{p,+}(\cdot)$ and $h_{p,-}(\cdot)$, and to extend the model to a non-autonomous system by incorporating rainfall and drainage as external inputs [20], while also examining its long-term stability and robustness against external disturbances.

ACKNOWLEDGMENT

This work was supported by JSPS KAKENHI Grant Numbers JP22H00512 and JP24K21314.

REFERENCES

[1] N. W. Arnell and S. N. Gosling, "The impacts of climate change on river flood risk at the global scale," *Climatic Change*, vol. 134, no. 3, pp. 387–401, 2016.

[2] H. Alifu, Y. Hirabayashi, Y. Imada, and H. Shiogama, "Enhancement of river flooding due to global warming," *Scientific Reports*, vol. 12, p. 20 687, 2022.

[3] V. P. Singh, S. K. Jain, and M. M. Sherif, "Errors of kinematic wave and diffusion wave approximations for time-independent flows with infiltration and momentum exchange included," *Hydrological Processes*, vol. 19, pp. 1771–1790, 2005.

[4] C. H. David, J. M. Hobbs, M. J. Turmon, C. M. Emery, J. T. Reager, and J. S. Famiglietti, "Analytical propagation of runoff uncertainty into discharge uncertainty through a large river network," *Geophysical Research Letters*, vol. 46, pp. 8102–8113, 2019.

[5] Y. Arai, S. Muramatsu, H. Yasuda, K. Hayasaka, and Y. Otake, "Sparse-coded dynamic mode decomposition on graph for prediction of river water level distribution," in *2021 IEEE International Conference on Acoustics, Speech and Signal Processing (ICASSP)*, 2021, pp. 3225–3229.

[6] M. O. Williams, I. G. Kevrekidis, and C. W. Rowley, "A data–driven approximation of the Koopman operator: Extending dynamic mode decomposition," *Journal of Nonlinear Science*, vol. 25, no. 6, pp. 1307–1346, Jun. 2015.

[7] C. Folkestad, D. Pastor, I. Mezic, R. Mohr, M. Fonoberova, and J. Burdick, *Extended dynamic mode decomposition with learned Koopman eigenfunctions for prediction and control*, 2020. arXiv: 1911.08751.

[8] A. Sakiyama, K. Watanabe, Y. Tanaka, and A. Ortega, "Two-channel critically sampled graph filter banks with spectral domain sampling," *IEEE Transactions on Signal Processing*, vol. 67, no. 6, pp. 1447–1460, Mar. 2019.

[9] F. Zhou, J. Z. Jiang, and P. L. Shui, "Optimization design of M-channel oversampled graph filter banks via successive convex approximation," *Circuits Syst. Signal Process.*, vol. 38, no. 10, pp. 4787–4798, Oct. 2019.

[10] R. Ito, T. Naito, H. Yasuda, M. Nagahara, and S. Muramatsu, "Sparse-coded time-delay graph DMD for prediction of river water level distribution," in *2024 International Technical Conference on Circuits/Systems, Computers, and Communications (ITC-CSCC)*, 2024, pp. 1–5.

[11] R. Ito, H. Kanauchi, T. Naito, H. Yasuda, M. Nagahara, and S. Muramatsu, "Sparse-coded time-delay graph DMD for nonlinear state-space modeling on graphs," *submitted to IEICE Transactions on Fundamentals of Electronics, Communications and Computer Sciences*, 2025, Manuscript under review.

[12] D. Dylewsky, E. Kaiser, S. L. Brunton, and J. N. Kutz, "Principal component trajectories for modeling spectrally continuous dynamics as forced linear systems," *Phys. Rev. E*, vol. 105, p. 015 312, 1 Jan. 2022.

[13] S. Furutani, T. Shibahara, M. Akiyama, K. Hato, and M. Aida, "Graph signal processing for directed graphs based on the hermitian laplacian," in *Lecture Notes in Computer Science*, ser. Lecture Notes in Artificial Intelligence and Bioinformatics, vol. 11906, 2020, pp. 447–463.

[14] H. Kitamura, H. Yasuda, Y. Tanaka, and S. Muramatsu, "Realization of digraph filters via augmented GFT," in *2023 IEEE International Conference on Image Processing (ICIP)*, 2023, pp. 2885–2889.

[15] S. Kwak, L. Shimabukuro, and A. Ortega, "Frequency analysis and filter design for directed graphs with polar decomposition," in *2024 IEEE International Conference on Acoustics, Speech and Signal Processing (ICASSP)*, 2024, pp. 9661–9665.

[16] T. Naito, R. Ito, Y. Tanaka, and S. Muramatsu, "Dictionary learning for directed graph signals via augmented GFT," *2024 Asia Pacific Signal and Information Processing Association Annual Summit and Conference (APSIPA ASC)*, Dec. 2024.

[17] J. H. Tu, C. W. Rowley, D. M. Luchtenburg, S. L. Brunton, and J. N. Kutz, "On dynamic mode decomposition: Theory and applications," *Journal of Computational Dynamics*, vol. 1, no. 2, pp. 391–421, 2014.

[18] P. J. Schmid, "Dynamic mode decomposition of numerical and experimental data," *Journal of Fluid Mechanics*, vol. 656, pp. 5–28, 2010.

[19] I. Daubechies, M. Defrise, and C. Mol, "An iterative thresholding algorithm for linear inverse problems with a sparsity constrains," *Communications on Pure and Applied Mathematics*, vol. 57, Nov. 2004.

[20] R. Ito, H. Kanauchi, H. Yasuda, M. Nagahara, and S. Muramatsu, "Sparse-coded time-delay DMD with control for nonlinear state-space modeling on graphs," in *2025 Asia Pacific Signal and Information Processing Association Annual Summit and Conference (APSIPA ASC)*, 2025.